5th International Conference on Experimental Fluid Mechanics ICEFM 2018 Munich
Munich, Germany, July 2-4, 2018

Scaling of adverse-pressure-gradient turbulent boundary layers

Ramis Örlü[1]*, Carlos Sanmiguel Vila[2], Ricardo Vinuesa[1], Andrea Ianiro[2], Stefano Discetti[2], Philipp Schlatter[1]

[1] Linné FLOW Centre, KTH Mechanics, Royal Institute of Technology, Stockholm, Sweden

[2] Universidad Carlos III de Madrid, Aerospace Engineering Group, Leganés, Spain

* ramis@mech.kth.se

Abstract

In the study of zero-pressure-gradient (ZPG) turbulent boundary layers (TBLs), small-scale universality of the inner-scaled streamwise velocity fluctuations is a re-occurring feature and serves as the underlying assumption in e.g. spatial-resolution correction schemes for hot-wire anemometry measurements as well as prediction schemes for turbulence statistics. Recent studies have also extended this small-scale similarity to pressure-gradient (PG) TBLs in order to apply these schemes. The present investigation is based on new experiments in an APG TBL with streamwise-independent Clauser pressure-gradient parameter in order to exclude upstream history effects. Results allow to revisit this underlying assumption and indicate that the small-scale energy is in fact enhanced with increasing APG strength.

1 Introduction

The quest for a better understanding of turbulent boundary layers (TBLs) is one of the main research goals of the turbulence community for many decades. Wall-bounded turbulence appears in many relevant fluid-flow problems such as the flow around wings, land and sea vehicles, or in turbines, compressors. Simplified scenarios, such as the zero-pressure-gradient (ZPG) TBL developing over a flat plate, have been investigated extensively to understand the fundamental aspects of wall-bounded turbulence (Marusic et al., 2010c). Unfortunately, ZPG conditions are nearly never encountered in real-life applications; instead, the majority of flow problems are under the effect of complex varying pressure gradients. In particular, adverse pressure gradients (APGs) might produce flow separation with the consequent loss in performance (Vinuesa et al., 2017b). Under these conditions, the applicability of the knowledge from ZPG TBLs to decelerating boundary layers is still rather limited (Vinuesa et al., 2017a).

Part of the complexity associated to the study of TBLs under the influence of an APG is due to the wider parametric space with respect to its ZPG counterpart. An obvious additional parameter for the study of APG TBLs is the streamwise pressure gradient, commonly expressed in terms of the Clauser pressure-gradient parameter, $\beta = (\delta^*/\tau_w)(\mathrm{d}P/\mathrm{d}x)$ (Clauser, 1954), where δ^* is the displacement thickness, τ_w is the mean wall-shear stress, and $\mathrm{d}P/\mathrm{d}x$ the pressure gradient along the streamwise coordinate. However, as recently shown by Bobke et al. (2017), the local state of an APG TBL is strongly affected by its upstream history, implying that the TBL has a memory of its upstream conditions that is much more pronounced than that of inflow and tripping effects in ZPG TBLs (Sanmiguel Vila et al., 2017b). Recent efforts have therefore tried to accommodate the accumulated effect of β, as opposed to considering the local β alone when comparing various APG TBLs (Sanmiguel Vila et al., 2017a; Vinuesa et al., 2017a). In light of the difficulty to fully encompass the effect of upstream pressure-gradient effects in the study of APG TBLs, Clauser (1954) proposed to study boundary layers in which the value of β is maintained constant over some downstream extent such that the ratio of the pressure gradient force to the wall shear stress remains constant. This condition, according to Rotta (1962) and Mellor and Gibson (1966), is needed to reach a near-equilibrium state in which the mean velocity deficit in the outer part is expected to be self-similar at sufficiently high Reynolds numbers (Marusic et al., 2010c).

In the present study, we will – for the sake of simplicity – abstain from investigating pressure-gradient history effects, and instead focus on two near-equilibrium TBLs, i.e. a ZPG TBL ($\beta = 0$) and a APG TBL ($\beta \approx 1.1$) in order to discuss their scale-decomposed contribution to the streamwise velocity spectra and variance, and ultimately address whether the often assumed universality of the small-scale energy contribution is also persistent in APG TBLs. Such investigations have previously been hampered due to the low Reynolds numbers assessable in simulations (Bobke et al., 2017) and the mixed upstream (pressure-gradient) histories despite matched local pressure-gradient conditions (Monty et al., 2011). For this purpose, new wind-tunnel experiments have been performed, and streamwise velocity statistics have been collected by means of hot-wire anemometry supplemented by oil-film interferometry, which are described next.

2 Experimental set-up

The experiments were performed in the Minimum Turbulence Level (MTL) closed-loop wind tunnel located at KTH Royal Institute of Technology in Stockholm. The test section is 7 m long with a cross-sectional area of 0.8 $\times$ 1.2 m^2 (height $\times$ width). The boundary layer developed on a suspended flat plate of 6 m length that has a leading edge following the shape of a modified super ellipse. The plate was also equipped with a 1.5 m long trailing-edge flap in order to modify the position of the stagnation point, see Figure 1a). In the present experimental campaign, the flap position was set to 10°. For a more detailed description of the wind tunnel, the flat plate and the specific tripping used, the reader is referred to Sanmiguel Vila et al. (2017b).

Besides the ZPG conditions, three APG distributions were obtained in the experimental campaign by means of wall inserts made of foam and attached to the roof of the MTL. The design of the different pressure-gradient configurations was performed by an iterative process, starting from a non-constant mild pressure gradient ($\beta \approx 0.7$) and modifying this configuration to different non-constant configurations with values up to $\beta \approx 2.5$, and eventually reaching a constant $\beta \approx 1.1$ configuration as shown in Figure 1b). The first trial shape of the ceiling was designed by performing Reynolds-Averaged Navier–Stokes (RANS) computations by considering the two-equation Shear-Stress Transport (SST) model (Menter, 1994) implemented in the CFD code Fluent (v.6.3), as described in Vinuesa et al. (2014). A schematic of the different geometries used is represented in Figure 1a), where the converging-diverging shape of the different geometries can be appreciated. In all the configurations the flow was initially accelerated by reducing the tunnel test section height from 0.80 m to approximately 0.60 m. The flat plate was placed at a vertical distance of 0.42 m from the roof at the throat. The leading edge of the flat plate was located right at the beginning of the roof throat. Downstream of the leading edge of the flat plate, the ceiling geometry was designed such that a ZPG was maintained for approximately 1.0 m. From that location on, the different adverse-pressure-gradient conditions were imposed by changing the roof geometry in the divergent part. Modifications in the slope and shape of the divergent part of the geometry allowed to obtain a higher β by producing a larger expansion.

Streamwise velocity measurements were performed by means of home-made single hot-wire probes

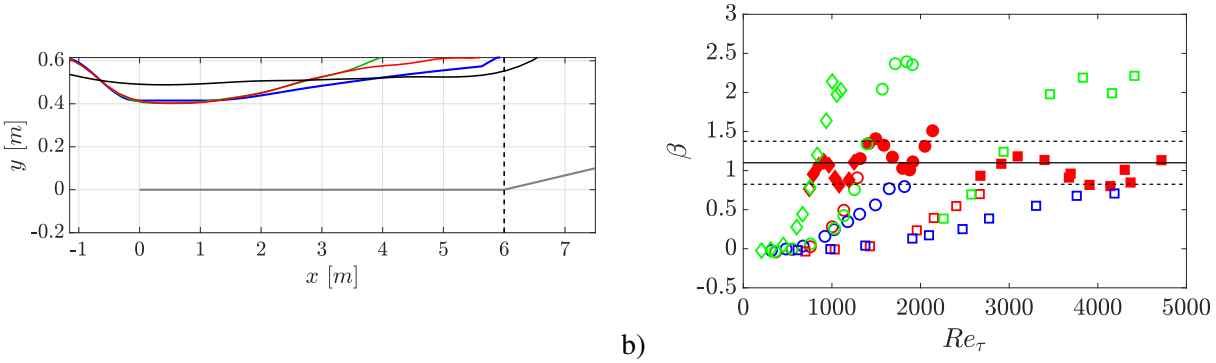

a) b)

Figure 1: a) Geometry of the roof and b) its Clauser pressure-gradient parameter β plotted as function of friction Reynolds number Re_τ: red (roof configuration 1), blue (roof configuration 2) and green (roof configuration 3). Gray line represents the aluminium flat plate used in the present experimental campaign. A ZPG configuration (i.e. $\beta \approx 0$) from Sanmiguel Vila et al. (2017b) (black line) has been included as a reference. Symbols correspond to: ($\diamond$) $U_{ref} = 6$ m/s, ($\circ$) $U_{ref} = 12$ m/s and ($\square$) $U_{ref} = 30$ m/s. Symbols are filled in the region bounded by 25% deviation from $\beta = 1.1$ is considered to be approximately constant.

which resemble a standard *Dantec* boundary-layer probe, *i.e.*, a 55P15. The hot-wire probes were etched using a stubless Platinum wire with lengths between 0.5–0.6 mm and nominal diameter of 2.5 and 1.25 μm. The wires were soldered to conical prongs with diameter of around 30 μm. Voltage signals from the hot-wire were recorded using a *Dantec StreamLine* 90N10 frame in conjunction with a 90C10 constant-temperature anemometer module operated at a resistance overheat of 80%. An offset and gain were applied to the top of the bridge voltage in order to match the voltage range of the 16-bit A/D converter used. All the measurements were recorded using a sampling duration with at least 20000 turn-over times (in term of TU_∞/δ_{99}, where T is the total sampling duration) and an acquisition frequency of around one viscous time unit. Calibration of the hot-wire was performed *in situ* using as reference a Pitot-static tube located parallel to the incoming free stream that was connected to a micromanometer of type *FC0510 (Furness Control Limited)*, which was also employed to record the ambient temperature and pressure during the calibration and experiments. Data acquired in the calibration was fitted to a fourth-order polynomial curve.

Oil-film interferometry (OFI) was used to measure the wall-shear stress at some locations and validate the process to determine the friction velocity based on near-wall velocity measurements as described in Chauhan et al. (2009). For further details on the performed OFI measurements at pressure gradient conditions, as well as on the post-processing of the data, the reader is referred to Vinuesa and Örlü (2016).

3 Results

In this section, we analyse the evolution of the different APG TBLs along the flat plate. In particular, the data sets are first presented in terms of their shape factor upon which the mean streamwise velocity profiles for the ZPG ($\beta = 0$) and APG with constant β-distribution, i.e. $\beta \approx 1.1$, are compared at two different Reynolds numbers in order to reveal Reynolds-number and pressure-gradient effects, without ambiguity due to different upstream histories. The comparison is then extended to the streamwise small- and large-scale decomposed variance profiles in light of their spectral energy distribution.

Figure 2a) shows the development of the shape factor H_{12} against the momentum-loss-based Reynolds number Re_θ. Although all three APG configurations are presented here, it is apparent that only the configuration that remains approximately constant in terms of β exhibits a trend that resembles that of the ZPG TBL, as previously observed in Vinuesa et al. (2017a), from which also the correlation for an APG with $\beta = 1$ (blue solid line) has been depicted in the same plot together with the correlation for a ZPG (black solid line) by Nagib et al. (2007). Since the APG TBLs develop from a ZPG, recall Figure 1, the transition from the canonical ZPG TBL state to that of a near-equilibrium APG can clearly be followed. Note that the slightly higher value of H_{12} for the intermediate freestream velocity is in accordance with the higher β values encountered in Figure 1b), while the lower and higher freestream velocity cases of the roof configuration 1 are in good agreement with the prediction by Vinuesa et al. (2017a) for $\beta = 1$. The streamwise mean velocity profile for the $\beta = 0$ and 1.1 for two selected friction Reynolds numbers of Re_τ =1900 and 4400 are shown

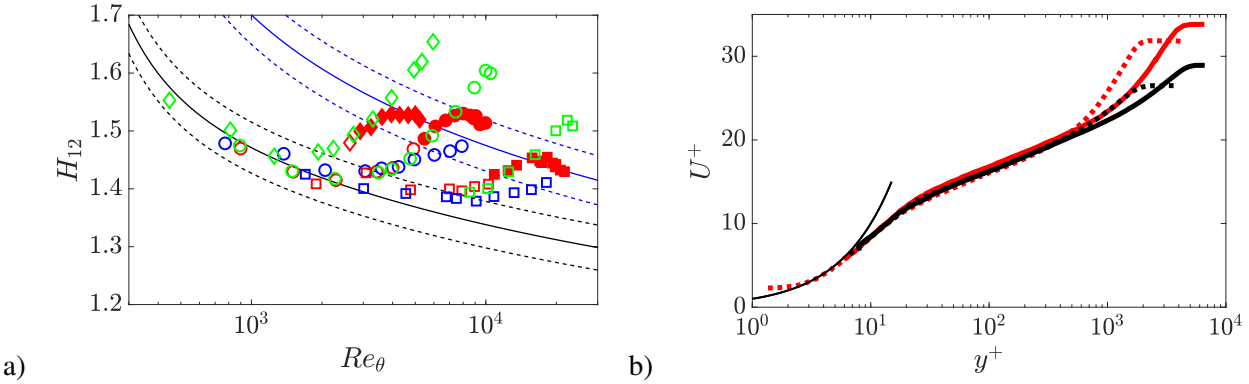

Figure 2: a) Reynolds-number evolution of the shape factor H_{12} as function of Re_θ, where the black and blue solid line are the ZPG and $\beta = 1$ correlations given by Chauhan et al. (2009) and Vinuesa et al. (2017a), respectively, together with their $\pm 3\%$ tolerances represented through dashed lines. b) Inner-scaled mean streamwise velocity, where ━ represents the reference ZPG ($\beta \approx 0$) and ━ the $\beta \approx 1.1$ case for $Re_\tau \approx 1900$ (dashed lines) and 4400 (solid lines).

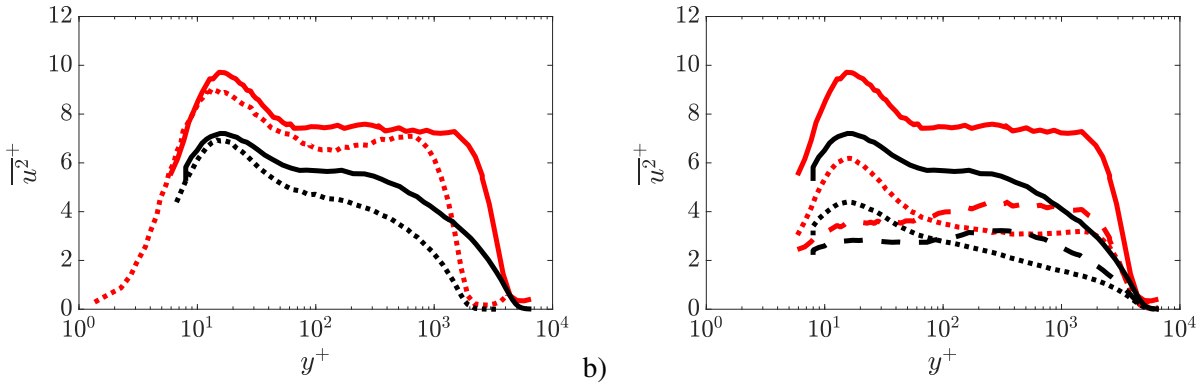

Figure 3: a) Inner-scaled streamwise variance profile for the ZPG (black lines) and APG (red lines) case for $Re_\tau \approx 1900$ (dashed lines) and 4400 (solid lines). b) The decomposed small- (dotted line) and large-scale (dashed line) contributions for the Re_τ =4400 case (solid line) shown in subplot a).

in Figure 1b) and indicate that the skin-friction coefficient (proportional to the inverse of the inner-scaled freestream velocity) of the APG cases remains parallel to its ZPG counterpart at a lower level.

Considering the corresponding streamwise variance profiles in Figure 3a) for the same cases shown in Figure 1b), the expected enhancement of the turbulence activity with both Reynolds number and pressure-gradient strength can be observed. It should be noted that the damped increase for the ZPG case around the near-wall peak, is an artifact of spatial resolution effects (Örlü and Alfredsson, 2013), in particular, at the higher Reynolds number. The outer region, instead, as well as the APG profiles, are, however, less effected by spatial resolution effects. While the emergence of an outer peak in the streamwise variance profile for ZPG TBLs at high Reynolds numbers is still debated (Alfredsson et al., 2011), its presence for APG TBLs even at relatively low Reynolds numbers is established (Bobke et al., 2017). The underlying mechanism for the existence of this outer peak is, however, different, since its location in ZPG TBLs is clearly within the logarithmic layer and close to the location of the Reynolds-shear stress maximum (Alfredsson et al., 2011), while it is an outer-layer phenomena (i.e. its location is encountered in the outer region) in case of APG TBLs. It should also be emphasised that the in increase of the inner-scaled variance can also not simply be related to the lower value of the skin friction, but can be ascribed to enhanced large-scale motions in the outer region (Harun et al., 2013).

One finding of previous studies was that the small-scale contribution remained essentially universal to pressure-gradient effects (see e.g. Harun et al., 2013) when scaled in inner units, besides its previously established Reynolds-number independence (Marusic et al., 2010a). While the latter could be confirmed also in our ZPG data (not shown here), there appears to be an enhancement of small-scale energy with increasing pressure-gradient strength as seen in Figure 3b). Note that Taylor's hypothesis is not utilized here to form the streamwise wavelength as commonly done in one-point experimental data Mathis et al. (2009)) and that the spectral maps and the spectral cut-off is defined in terms of time rather than streamwise wavelength. Based on previous results (Eitel-Amor et al., 2014), the cut-off has been applied at 400 viscous time units, which appears to be a reasonable compromise to effectively separate between the inner and outer peaks in the temporal spectra as apparent from the spectral maps in Figure 4.

While the small-scale energy in ZPGs scales throughout the entire boundary-layer thickness (Marusic et al., 2010a), it is clear that this does not extend to APG TBLs, where the small-scale energy contribution is also enhanced in the outer region, where spatial resolution effects are not to be expected (Örlü and Alfredsson, 2013). As recently shown in Dogan et al. (2018), the temporal filter is rather inefficient at low-to-moderate Reynolds numbers, hence some caution is advised here; however this is often the only possibility in single-point hot-wire measurements. Assuming that the scale-decomposed variances are representative, correction schemes for spatial resolution effects that consider the viscous length scale as the main parameter (such as the one by Smits et al., 2011) should thus be considered with caution for APG TBLs. This also implies that comparisons at (relatively large and) matched viscous-scaled hot-wire lengths (as is the case of Harun et al., 2013) will not ensure that there is no bias due to spatial resolution effects.

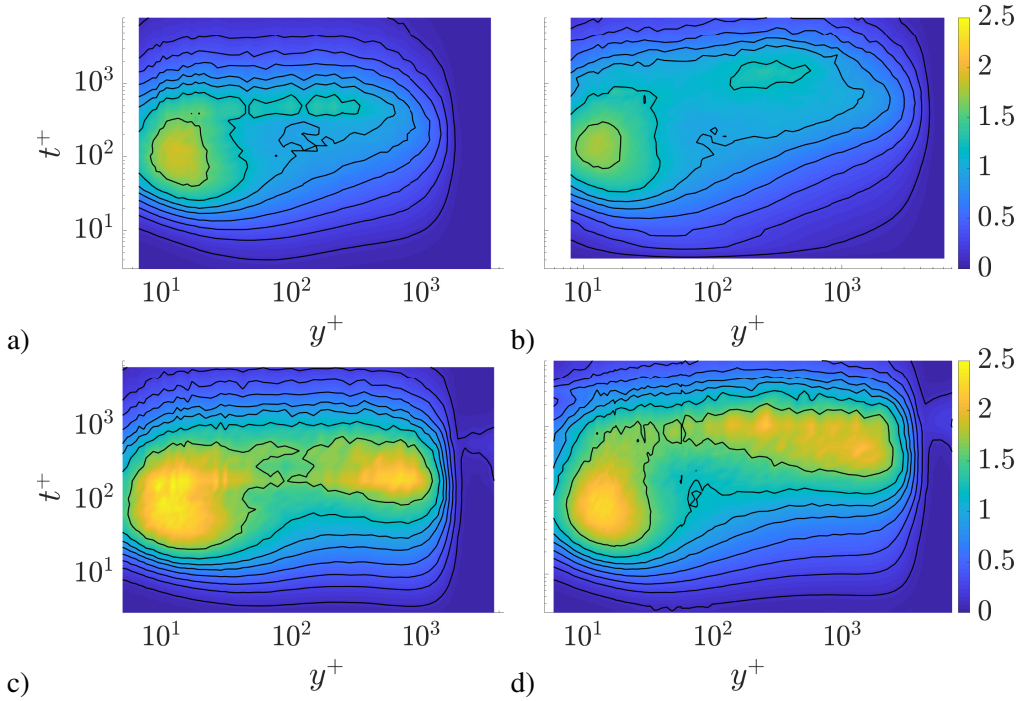

Figure 4: Contour map of the premultiplied energy spectra of the streamwise velocity with contour levels as fixed values of $f^+\Phi^+_{uu}$. ZPG ($\beta = 0$) for a) $Re_\tau \approx 1900$ and b) 4400. APG ($\beta \approx 1.15$) for c) $Re_\tau \approx 1900$ and d) 4400.

4 Conclusion

Single-point hot-wire anemometry measurements were performed in an adverse-pressure-gradient turbulent boundary layer with a streamwise-independent Clauser pressure-gradient parameter β in order to minimise the effect of upstream (pressure-gradient) effects. This allowed a fair comparison between a ZPG and APG in terms of small- and large-scale energy contributions to the streamwise variance profile. It was found that, contrary to previous studies, the small-scale energy contribution is not universal, but dependent on the pressure-gradient strength, which has direct implications on correction schemes for measurement techniques as well as predictions that are based on small-scale universality (Marusic et al., 2010b) when extended towards pressure-gradient turbulent boundary layers. Further studies will be required to ensure that the findings are not biased by the deficiencies of the temporal cut-off filter for the scale separation.

Acknowledgements

RÖ, RV and PS acknowledge the financial support from the Lundeqvist foundation, Swedish Research Council (VR) and the Knut and Alice Wallenberg Foundation. CSV, SD and AI were partially supported by the COTURB project (Coherent Structures in Wall-bounded Turbulence), funded by the European Research Council Coturb Grant No. ERC-2014.AdG-669505.

References

Alfredsson PH, Segalini A, and Örlü R (2011) A new scaling for the streamwise turbulence intensity in wall-bounded turbulent flows and what it tells us about the "outer" peak. *Phys Fluids* 23:041702

Bobke A, Vinuesa R, Örlü R, and Schlatter P (2017) History effects and near equilibrium in adverse-pressure-gradient turbulent boundary layers. *J Fluid Mech* 820:667–692

Chauhan KA, Monkewitz PA, and Nagib HM (2009) Criteria for assessing experiments in zero pressure gradient boundary layers. *Fluid Dyn Res* 41:021404

Clauser FH (1954) Turbulent boundary layers in adverse pressure gradients. *J Aero Sci* 21:91–108

Dogan E, Örlü R, Gatti D, Vinuesa R, and Schlatter P (2018) Quantification of amplitude modulation in wall-bounded turbulence. *Fluid Dynamics Research, DOI: 101088/1873-7005/aaca81*

Eitel-Amor G, Örlü R, and Schlatter P (2014) Simulation and validation of a spatially evolving turbulent boundary layer up to $Re_\theta = 8300$. *Int J Heat Fluid Flow* 47:57–69

Harun Z, Monty JP, Mathis R, and Marusic I (2013) Pressure gradient effects on the large-scale structure of turbulent boundary layers. *J Fluid Mech* 715:477–498

Marusic I, Mathis R, and Hutchins N (2010a) High Reynolds number effects in wall turbulence. *Int J Heat Fluid Flow* 31:418–428.

Marusic I, Mathis R, and Hutchins N (2010b) Predictive model for wall-bounded turbulent flow. *Science* 329:193–196

Marusic I, McKeon BJ, Monkewitz PA, Nagib HM, Smits AJ, and Sreenivasan KR (2010c) Wall-bounded turbulent flows at high Reynolds numbers: Recent advances and key issues. *Phys Fluids* 22:065103

Mathis R, Hutchins N, and Marusic I (2009) Large-scale amplitude modulation of the small-scale structures in turbulent boundary layers. *J Fluid Mech* 628:311–337

Mellor G and Gibson D (1966) Equilibrium turbulent boundary layers. *J Fluid Mech* 24:225–253

Menter FR (1994) Two-equation eddy-viscosity turbulence models for engineering applications. *AIAA J* 32:1598–1605

Monty JP, Harun Z, and Marusic I (2011) A parametric study of adverse pressure gradient turbulent boundary layers. *Int J Heat Fluid Flow* 32:575–585

Nagib HM, Chauhan KA, and Monkewitz PA (2007) Approach to an asymptotic state for zero pressure gradient turbulent boundary layers. *Phil Trans R Soc A* 365:755–770

Örlü R and Alfredsson PH (2013) On spatial resolution issues related to time-averaged quantities using hot-wire anemometry. *Exp Fluids* 54:1431

Rotta J (1962) Turbulent boundary layers in incompressible flow. *Progress in Aerospace Sciences* 2

Sanmiguel Vila C, Örlü R, Vinuesa R, Schlatter P, Ianiro A, and Discetti S (2017a) Adverse-pressure-gradient effects on turbulent boundary layers: Statistics and flow-field organization. *Flow Turbul Combust* 99:589–612

Sanmiguel Vila C, Vinuesa R, Discetti S, Ianiro A, Schlatter P, and Örlü R (2017b) On the identification of well-behaved turbulent boundary layers. *J Fluid Mech* 822:109–138

Smits AJ, Monty JP, Hultmark M, Bailey SCC, Hutchins N, and Marusic I (2011) Spatial resolution correction for wall-bounded turbulence measurements. *J Fluid Mech* 676:41–53

Vinuesa R and Örlü R (2016) Measurement of wall shear stress. in S Discetti and A Ianiro, editors, *Experimental Aerodynamics*. pages 393–428. CRC Press Taylor & Francis Group

Vinuesa R, Örlü R, Sanmiguel Vila C, Ianiro A, Discetti S, and Schlatter P (2017a) Revisiting history effects in adverse-pressure-gradient turbulent boundary layers. *Flow Turbul Combust* 99:565–587

Vinuesa R, Örlü R, and Schlatter P (2017b) Characterisation of backflow events over a wing section. *J Turbulence* 18:170–185

Vinuesa R, Rozier PH, Schlatter P, and Nagib HM (2014) Experiments and computations of localized pressure gradients with different history effects. *AIAA J* 52:368–384